Biochimica et Biophysica Acta 1808 (2011) 642–648

Contents lists available at ScienceDirect

Biochimica et Biophysica Acta

journal homepage: www.elsevier.com/locate/bbamem

Membrane hydraulic permeability changes during cooling of mammalian cells

Maryam Akhoondi [a], Harriëtte Oldenhof [b], Christoph Stoll [a], Harald Sieme [b], Willem F. Wolkers [a,*]

[a] Institute of Multiphase Processes, Leibniz Universität Hannover, Hannover, Germany
[b] Clinic for Horses - Unit for Reproductive Medicine, University of Veterinary Medicine Hannover, Hannover, Germany

ARTICLE INFO

Article history:
Received 3 October 2010
Accepted 18 November 2010
Available online 30 November 2010

Keywords:
Fourier transform infrared spectroscopy
Lipid phase behavior
Suprazero and subzero membrane hydraulic permeability
Cryobiology

ABSTRACT

In order to predict optimal cooling rates for cryopreservation of cells, the cell-specific membrane hydraulic permeability and corresponding activation energy for water transport need to be experimentally determined. These parameters should preferably be determined at subzero temperatures in the presence of ice. There is, however, a lack of methods to study membrane properties of cells in the presence of ice. We have used Fourier transform infrared spectroscopy to study freezing-induced membrane dehydration of mouse embryonic fibroblast (3T3) cells and derived the subzero membrane hydraulic permeability and the activation energy for water transport from these data. Coulter counter measurements were used to determine the suprazero membrane hydraulic permeability parameters from cellular volume changes of cells exposed to osmotic stress. The activation energy for water transport in the ice phase is about three fold greater compared to that at suprazero temperatures. The membrane hydraulic permeability at 0 °C that was extrapolated from suprazero measurements is about five fold greater compared to that extrapolated from subzero measurements. This difference is likely due to a freezing-induced dehydration of the bound water around the phospholipid head groups. Using Fourier transform infrared spectroscopy, two distinct water transport processes, that of free and membrane bound water, can be identified during freezing with distinct activation energies. Dimethylsulfoxide, a widely used cryoprotective agent, did not prevent freezing-induced membrane dehydration but decreased the activation energy for water transport.

1. Introduction

Cryopreservation relies on ultra low temperatures to store cells for prolonged periods. Cooling and re-warming, however, can be damaging to cells. For cells undergoing freezing, a two-factor hypothesis of damage has been developed (for review, see reference 1). At high cooling rates, cell losses are associated with intracellular ice formation. For cells cooled slowly, damage is described as 'solution effects injury,' which is related to cellular dehydration. Typically, there is a critical cooling rate for maximum survival. This cooling rate, however, varies greatly depending upon the cell type and is related to cell-specific membrane properties. A rational design of cryopreservation protocols for cells requires understanding of the membrane phase and permeability changes that take place during cooling and warming at supra and subzero temperatures.

Theoretical models have been developed to describe the transport of water across the cell membrane at subzero temperatures [2–4]. These models describe cellular volume changes during freezing as a function of cell dimensions and membrane permeability parameters. In turn, once cell-specific membrane hydraulic permeability parameters are known, they can be used to predict the cellular response (i.e. dehydration or intracellular ice formation) under different freezing conditions. The membrane permeability to water can be determined at suprazero temperatures by exposure of cells to osmotic stress but should preferably be determined at subzero temperatures using different cooling regimes [3]. There is, however, a lack of experimental methods that can be used to determine subzero membrane permeability parameters.

Cryomicroscopy and differential scanning calorimetry (DSC) are currently being used as the standard methods to derive subzero membrane permeability parameters. The extent of mechanistic information that can be derived using these techniques, however, is limited. Cryomicroscopy can only be used to detect cell volume changes or intracellular ice formation [5–7]. Membrane properties are not measured directly. In addition, cryomicroscopy can only be used for sufficiently large and spherical cells. DSC can be used to derive subzero membrane permeability parameters of non-spherical small cells (i.e. sperm) and tissues [8–11], based on the latent heat release of the water-to-ice phase change during freezing of cell pellets. DSC is a bulk scale technique that does not provide mechanistic information with regard to the effects on specific cellular structures.

Abbreviations: E_{Lp}, activation energy of the cell membrane permeability to water; FTIR, Fourier transform infrared spectroscopy; Lp, membrane hydraulic permeability; Lpg, membrane hydraulic permeability at 0 °C; Tn, ice nucleation temperature; V_o, isosmotic cell volume; V_b, osmotically inactive cell volume

* Corresponding author. Institute of Multiphase Processes, Leibniz Universität Hannover, Callinstrasse 36, 30167 Hannover, Germany. Tel.: +49 511 762 19353; fax: +49 511 762 19389.
E-mail addresses: wolkers@imp-uni-hannover.de, wolkers@yahoo.com (W.F. Wolkers).

0005-2736/$ – see front matter © 2010 Elsevier B.V. All rights reserved.
doi:10.1016/j.bbamem.2010.11.021

The limitations of cryomicroscopy and DSC have prompted the development of new methods such as Fourier transform infrared spectroscopy (FTIR) to study cells at subzero temperatures. We have recently shown how FTIR can be used to study subzero membrane phase behavior of mammalian cells from which subzero membrane hydraulic permeability parameters can be derived [12–14]. FTIR provides greater detail on water transport processes during freezing of cells compared to DSC or cryomicroscopy since it allows for direct assessment of changes in biomolecular interactions and structures in cells during cooling. Using FTIR, two water transport processes were identified during freezing of sperm: that of free and that of membrane bound water [14].

The basis for FTIR studies on lipids and proteins in cells is that endogenous biomolecules have characteristic molecular group vibrations. Temperature-dependent acquisition of FTIR spectra of cells can be used to derive information on molecular conformation and inter-molecular interactions of biomolecules in their native environment during cooling or warming. Lipid phase transitions in isolated biological membranes and in whole cells can be monitored using the CH_2 stretching vibrations arising from the lipid acyl chains [15–17]. FTIR is particularly suitable for cryobiological research because it can be used to measure hydrated as well as frozen systems [18].

Our understanding of how cryoprotectants preserve cellular membranes and proteins during cooling and re-warming is limited. The stabilizing effect of cryoprotective agents has been explained by the preferential exclusion mechanism [19], which states that cryoprotectants stabilize biomolecules because they are preferentially excluded from biomolecular surfaces thereby stabilizing the native state. Although it is believed that the preferential exclusion mechanism can be extrapolated during freezing, experimental evidence for this is lacking. We have recently shown that glycerol does not prevent lyotropic membrane phase transitions during freezing of stallion sperm [14]. It controls the rate at which water is removed from phospholipid head groups of cellular membranes.

In this study, the membrane hydraulic permeability of mouse embryonic fibroblast (3T3) cells was determined at supra as well as subzero temperatures. Coulter counter measurements were done to determine the osmotic active and inactive volume of the cells. The membrane hydraulic permeability was determined at various temperatures from volume measurements upon exposure of the cells to hyperosmotic conditions. FTIR was used to study subzero membrane phase behavior and to determine the membrane permeability to water in the presence of ice. In addition, the effect of the cryoprotectant dimethylsulfoxide (DMSO) on subzero membrane properties was studied. The obtained membrane permeability values were plotted in an Arrhenius plot to compare the activation energy for water transport above and below the water-to-ice transition.

2. Materials and methods

2.1. Cell culture conditions

3T3 cells were cultured in T75-flasks (Biochrom, Berlin, Germany) under sterile conditions. Cultures were grown in Dulbecco's Modified Eagle Medium supplemented with 10% fetal bovine serum and 100 U/mL penicillin/streptomycin (Biochrom, Berlin, Germany) at 37 °C under 5% CO_2 for 3 days, after which they were transferred into fresh medium. Cells were harvested after reaching 70%–80% confluency. Cells were trypsinized with 2 mL 0.25% (vol./vol.) trypsin for 3 min, centrifuged at 1000*g* for 8 min at 4 °C and re-suspended in culture medium. Cell pellets for FTIR analysis were obtained by centrifugation at 1400*g* for 1 min at 4 °C. For incubations in the presence of the cryoprotectant dimethylsulfoxide, DMSO (Carl Roth, Karlsruhe, Germany) was added dropwise to a final concentration of 5% (vol./vol.) while keeping the cells on ice. Cells were incubated for 10 min on ice to allow for DMSO diffusion, after which cell pellets for FTIR analysis were obtained as described above.

2.2. Assessment of suprazero osmotic properties

Cell size distributions were determined using a Beckman-Coulter Multisizer III (Coulter Corporation, Fullerton, CA, USA), equipped with an aperture of 100 μm in diameter. Isoton was used as electrolyte solution. For each (an)isosmotic condition tested, volume calibration was performed using beads with a diameter of 10 μm (Sigma-Aldrich, St. Louis, MO, USA).

For measurements under isosmotic conditions, cells were incubated in HEPES buffered saline solution (HBS) of 300 mOsm kg^{-1} (20 mM HEPES pH 7.4, 137 mM NaCl, 10 mM glucose, 2.5 mM KOH). Hypotonic solutions were prepared by diluting HBS with water. Hypertonic solutions were prepared by adding NaCl to HBS. The osmolality of the solutions was measured using an Osmomat 030 cryoscopic osmometer (Gonotec, Berlin, Germany). Hundred microliter cell suspension was added to ten milliliter (an)isosmotic HBS solution, and cells were incubated for ten minutes after which average cell volumes were determined from the size distributions of approximately 10,000 cells. Boyle van ´t Hoff relationships were established by plotting the normalized cell volumes at different osmotic solutions against the reciprocal of the osmolalities of these solutions. The osmotically inactive volume, V_b, of the cells was estimated by extrapolating a linear regression through the data points to the *y*-axis.

2.3. Estimation of suprazero Lp values

Water permeability coefficients (Lp) were determined from volume measurements upon exposure to anisosmotic conditions at various temperatures. Hundred microliter cell suspension was added to ten milliliter HBS solution of a particular osmolality (250, 500 or 1000 mOsm kg^{-1}) that was equilibrated at a particular temperature (*T*: 37, 25, or 8 °C) and cell volumes were recorded during ten minutes, using the Coulter counter described above. The data were fitted using the following equation, which describes the decrease in cell volume with time (dV/dt) due to water movement across the cell membrane [20]:

$$\frac{dV}{dt} = \mathrm{Lp}ART(\Delta C) \quad (1)$$

where *A* is the surface area for water transport, *R* the universal gas constant and ΔC the osmotic gradient between the intracellular and extracellular environment. Matlab software (Mathworks, Ismaning, Germany) was used to fit experimental data to Eq. (1), using the simplex method with Runge–Kutta numerical integration. The estimated Lp values at different temperatures were plotted in an Arrhenius plot to derive the activation energy for water transport (E_{Lp}) and to extrapolate Lp at 0 °C (Lpg).

2.4. Fourier transform infrared spectroscopy studies

Infrared absorption measurements were carried out with a Perkin-Elmer 100 Fourier transform infrared (FTIR) spectrometer (Perkin-Elmer, Norwalk, CT, USA), equipped with a narrow band mercury/cadmium/telluride liquid nitrogen cooled IR-detector. The optical bench was continuously purged with dry air from an FTIR purge gas generator (Whatman, Clifton, NJ, USA). The acquisition parameters were 4 cm^{-1} resolution, 8 co-added interferograms, 4000–900 cm^{-1} wavenumber range. Spectra analysis and display were carried out using Perkin-Elmer software (Perkin-Elmer,

Norwalk, CT, USA) and Omnic software (Thermo-Nicolet, Madison, WI, USA). Data analysis on membrane phase behavior and ice formation during freezing was done as previously described in detail [14]. Briefly, second derivative spectra were obtained using a 13 point smoothing factor. Membrane conformational disorder was monitored by observing the position of the CH_2 symmetric stretching band at approximately 2850 cm^{-1} (νCH_2), and wavenumber versus temperature plots were constructed for different ice nucleation conditions. Ice formation was monitored by following the position and area of the H_2O-libration and -bending band at approximately 2200 cm^{-1} ($A\nu H_2O$). Ice nucleation temperatures (Tn) were determined as the onset-point at which the H_2O band area sharply increased from $A\nu H_2O$ versus temperature plots.

2.5. Cooling conditions and induction of ice nucleation

For temperature-dependent FTIR measurements, a variable temperature FTIR sample holder with heater device (Harrick Scientific Products, Pleasantville, NY, USA) together with a Linkam pump system for using liquid nitrogen as a coolant (Linkam Scientific Instruments, Tadworth, Surrey, UK) was used. The sample temperature was monitored using a thermocouple that was located close to the sample. Cooling scans were performed in which the temperature was decreased from 20 °C to −40 °C at 1 °C min^{-1}. Spectra were acquired every 20 s. Generally, under the conditions used during this study, stochastic nucleation of the sample was around −14 °C. Higher nucleation temperatures were induced by touching the sample edge using a copper wire that was cooled using liquid nitrogen.

2.6. Water transport model during freezing

The reduction in cellular volume that occurs during freezing has been described by the water transport model [2–4]. The water transport model was further modified to incorporate the effect of cryoprotectants on the volumetric shrinkage response of cells during freezing [9,21]:

$$\frac{dV}{dT} = \frac{L_p ART}{v_w B}\left[ln\left(\frac{\left(V_o - V_b - n_{cpa}v_{cpa}\right)}{\left(V_o - V_b - n_{cpa}v_{cpa}\right) + v_w\left(v_s n_s + n_{cpa}\right)}\right) - \frac{\Delta H_f}{R}\left(\frac{1}{T_R} - \frac{1}{T}\right)\right] \quad (2)$$

Table 1
Parameters and variables for Eqs. (1) and (2). Dimensions of 3T3 cells were obtained from Coulter counter measurements.

Symbol	Description	Value	SI unit
V	Volume	(Variable)	m^3
T	Temperature	(Variable)	K
T_R	Reference temperature	273.15	K
Lp	Membrane hydraulic permeability	(Variable)	$ms^{-1}\,Pa^{-1}$
Lpg	Permeability of the membrane to water at T_R	(Parameter)	$ms^{-1}\,Pa^{-1}$
E_{Lp}	Activation energy for the permeation process	(Parameter)	$J\,mol^{-1}$
A	Membrane surface area of the cell	781×10^{-12}	m^2
R	Universal gas constant	8.314	$JK^{-1}\,mol^{-1}$
B	Cooling rate	0.0167	Ks^{-1}
v_w	Molar volume of water	18×10^{-6}	$m^3\,mol^{-1}$
V_o	Isotonic volume	2053×10^{-18}	m^3
V_b	Osmotically inactive volume	1068×10^{-18}	m^3
v_s	Dissociation constant of salt	2	(–)
n_s	Number of moles of solutes in the cell	5.694×10^{-15}	mol
n_{cpa}	Number of moles of CPA (DMSO) in the cell	$6.59\cdot10^{-13}$	mol
v_{cpa}	Molar volume of CPA (DMSO)	71×10^{-6}	$m^3\,mol^{-1}$
ΔH_f	Heat of fusion of water	6011	$J\,mol^{-1}$

Parameters and variables are summarized in Table 1. In this equation, the permeability of the plasma membrane to water (Lp in $m\,s^{-1}\,Pa^{-1}$) is defined by:

$$Lp = Lpg\ exp\left(-\frac{E_{Lp}}{R}\left(\frac{1}{T} - \frac{1}{T_R}\right)\right) \quad (3)$$

where Lpg is the membrane hydraulic permeability at 0 °C, and E_{Lp} represents the temperature dependence of the membrane permeability (activation energy, in $J\,mol^{-1}$). Dimensions of 3T3 cells were determined using Coulter counter measurements as described above.

2.7. Conversion of FTIR data in cell volume changes and determination of membrane permeability parameters

Cell volume normalization of νCH_2 versus temperature plots was done as previously described [14]. It was assumed that the freezing-induced shift in νCH_2 is proportional to the reduction in cellular volume that occurs due to water transport out of the cell in response to freezing. This means that the maximum shift in νCH_2 as attained with the highest subzero nucleation temperature at which the sample can be nucleated corresponds to maximum cellular dehydration (equals V_b) and partial dehydration is scaled relative to this. The band position of the lipid band (νCH_2) is related to cell volume changes during freezing by the following equation:

$$\frac{V(T)}{V_o} = 1 - \left(\frac{\upsilon CH_{2,o} - \upsilon CH_2(T)}{\upsilon CH_{2,o} - \upsilon CH_{2,max}}\right)\left(\frac{V_o - V_b}{V_o}\right) \quad (4)$$

where $V(T)$ represents the cell volume at a given temperature. Furthermore, $\nu CH_{2,o}$ is νCH_2 at the onset of ice nucleation (Tn), $\nu CH_2(T)$ is νCH_2 at a given temperature and $\nu CH_{2,max}$ is the νCH_2 as attained at −40 °C for the highest subzero nucleation temperature possible (condition that results in the maximum shift in νCH_2). The normalized volume (V/V_o) is assumed to be 1 just before freezing-induced dehydration (at Tn); relative shifts in νCH_2 were therefore calculated from Tn down to −40 °C.

Cellular dehydration can also be quantified using the H_2O-libration and -bending combination band: ice formation and cellular dehydration results in an increase in the area of this band [14]. Analogous to the method described for volume scaling of νCH_2 data, the area of the water band ($A\nu H_2O$) was converted into cell volumetric changes. The area of the water band ($A\nu H_2O$) is related to cell volume changes during freezing by the following equation:

$$\frac{V(T)}{V_o} = 1 - \left(\frac{A\upsilon H_2O_{,o} - A\upsilon H_2O(T)}{A\upsilon H_2O_{,o} - A\upsilon H_2O_{,max}}\right)\left(\frac{V_o - V_b}{V_o}\right) \quad (5)$$

where $A\nu H_2O_{,o}$ is the area of the H_2O band at the onset of ice nucleation, $A\nu H_2O(T)$ the area of the H_2O band at a given temperature and $A\nu H_2O_{,max}$ the $A\nu H_2O$ as attained at −40 °C for the highest subzero nucleation temperature possible.

Lp values at subzero temperatures were determined from cell volume scaled νCH_2 and $A\nu H_2O$ versus temperature plots. For a particular nucleation temperature, the slope dV/dT at nucleation was determined from cell volume versus temperature plots. dV/dT was used to determine Lp using Eq. (1). The natural logarithm of Lp was plotted as a function of the inverse of the nucleation temperature in an Arrhenius plot, which was used to derive the apparent activation energy (E_{Lp}) and the reference membrane hydraulic permeability at 0 °C (Lpg).

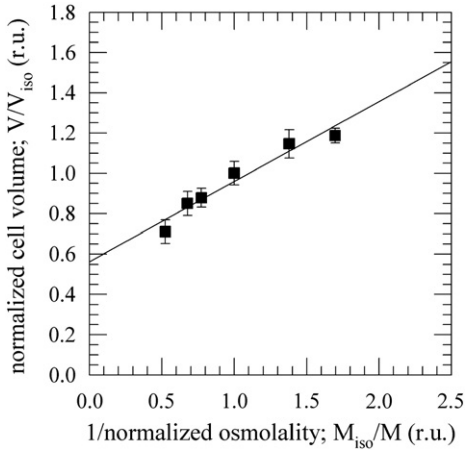

Fig. 1. Boyle van ´t Hoff relationship of 3T3 cells. The osmotic inactive volume was determined to be 56% of V_o.

3. Results

3.1. Boyle van ´t Hoff behavior

In order to determine the isosmotic volume as well as the osmotic inactive volume of 3T3 cells, cell volumes were determined by Coulter counter measurements after incubation in (an)isotonic media for 10 min. The cell volume in isotonic medium, V_o, was determined to be $2053 \pm 120\ \mu m^3$. Fig. 1 shows a Boyle van ´t Hoff plot of the cell volume data. The cells behave as linear osmometers in the investigated osmotic range (200–600 mOsm kg^{-1}). The osmotic inactive volume, V_b, that was obtained from extrapolation to infinite osmolality (the intercept of the linear regression line with the *y*-axis) was determined to be 56% of V_o.

3.2. Suprazero membrane permeability parameters for 3T3 cells

In order to determine the suprazero membrane permeability to water, volume changes of cells exposed to anisotonic media were recorded by Coulter counter measurements. Fig. 2A shows volume normalized plots of the cells upon exposure in hypo, iso and hypertonic media at room temperature. Cells shrink upon exposure to hypertonic media and swell upon exposure to hypotonic media. Cell volume reaches a plateau within 30 s. In order to determine the activation energy of Lp (E_{Lp}), the cell volume response in HBS of 500 mOsm kg^{-1} was measured at various temperatures ranging from 37 to 8 °C. Lp values were estimated from these data and plotted in an Arrhenius plot (Fig. 2B). The activation energy in the suprazero temperature regime was determined to be 15.0 kcal mol^{-1}, with an extrapolated value of Lp at 0 °C (Lpg) of 0.0631 μm min^{-1} atm^{-1}.

3.3. In situ FTIR studies during freezing of 3T3 cells

Fig. 3A shows in situ infrared spectra of 3T3 cells during freezing from 20 to −40 °C at a cooling rate of 1 °C min^{-1}. Bands arising from H_2O are visible at 3300 (OH-stretching), 2200 (H_2O-libration and -bending combination) and 1650 cm^{-1} (H_2O scissoring band). The CH stretching region (3000–2800 cm^{-1}) contains the asymmetric and symmetric membrane lipid CH_2 stretching vibration bands at 2929 and 2852 cm^{-1}, respectively. The symmetric CH_2 stretching band was used to monitor membrane phase behavior during freezing. The H_2O-libration and -bending combination band was used to determine ice formation during cooling of the sample. The spectral bands exhibit drastic shape changes upon ice formation.

3.4. Subzero membrane phase behavior in the absence and presence of DMSO

Fig. 3B shows membrane phase behavior and ice formation of cells during cooling from 20 to −40 °C at 1 °C min^{-1}. Ice formation, which was actively induced at a Tn of −2 °C, is visible from the H_2O band area (open symbols) as an abrupt increase in band area. The band position of the symmetric CH_2 stretching band (νCH_2), which provides a measure for the membrane conformational disorder, decreases with decreasing temperature and displays a drastic decrease upon ice formation indicating that ice formation causes membranes to undergo a fluid-to-gel phase transition. Dependent on the nucleation temperature to which cell pellets were exposed, membranes show different phase behavior (Fig. 4). At high nucleation temperatures, at a Tn of −2 °C, membranes undergo a profound membrane phase transition upon ice formation to a more ordered gel phase. By contrast, at a Tn of −14 °C, membranes undergo a smaller and more gradual decrease in membrane conformational disorder and remain relatively fluid. Intermediate membrane phase behavior is observed at a Tn of −4 °C.

Fig. 5A shows νCH_2 versus temperature plots in the presence and absence of DMSO, for high and low subzero nucleation temperature conditions. DMSO does not prevent freezing-induced membrane phase changes. Moreover, the freezing-induced fluid-to-gel

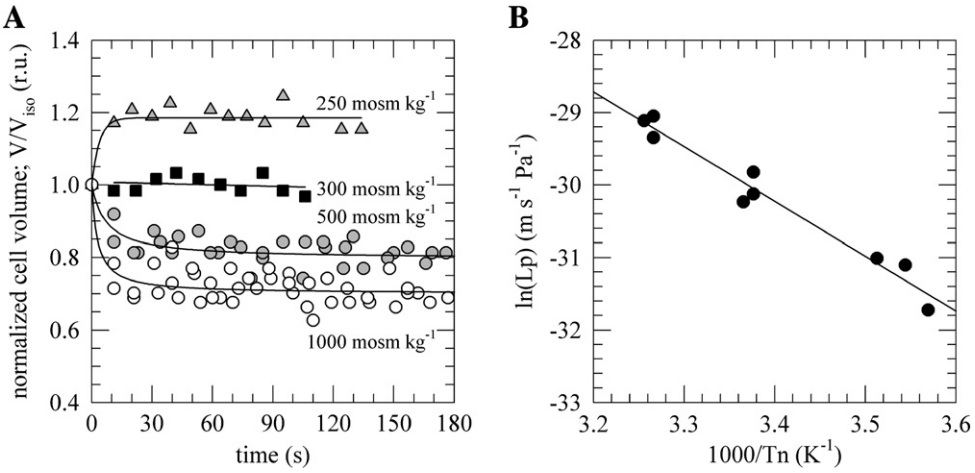

Fig. 2. (A) Osmotic response of 3T3 cells in anisotonic media. (B) Arrhenius plot of Lp determined from exposure of the cells to 500 mOsm kg^{-1} at various temperatures.

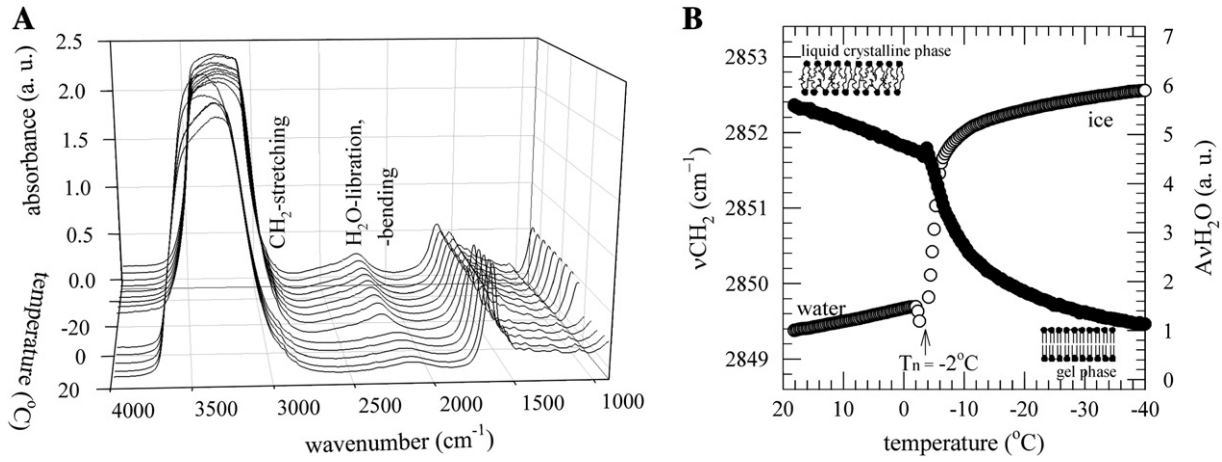

Fig. 3. 3D representation of FTIR spectra of 3T3 cells acquired during cooling from 20 °C to −40 °C at a cooling rate of 1 °C min^{-1} and nucleating the sample at −2 °C. Panel B shows membrane phase behavior (filled circles) and ice formation (open circles) during cooling of the sample in one plot. The data points reflect the band position of the lipid symmetric CH_2 stretching band (νCH_2) and the area of the H_2O-libration and -bending band ($A\nu H_2O$) as a function of the temperature, Tn is indicated with an arrow.

membrane phase transition is more gradual in the presence of DMSO and occurs over a wider temperature range.

3.5. Subzero membrane permeability parameters of 3T3 cells

The membrane phase behavior was studied in detail at different nucleation temperatures and used to determine Lp at subzero temperatures. The obtained membrane permeability values in the absence and presence of DMSO are plotted in an Arrhenius plot (Fig. 5B) to determine the activation energy and to extrapolate Lp at 0 °C. DMSO clearly affects the Lp values. In the absence of DMSO, $E_{Lp,subzero,bound\ water}$ and $Lpg_{subzero,bound\ water}$ were determined to be 44.1 kcal mol^{-1} and 0.0130 μm min^{-1} atm^{-1}, respectively. In the presence of DMSO, $E_{Lp,subzero,bound\ water,DMSO}$ and $Lpg_{subzero,bound\ water,DMSO}$ were determined to be 18.7 kcal mol^{-1} and 0.0044 μm min^{-1} atm^{-1}, respectively.

The H_2O band was analyzed similarly as the νCH_2 band to obtain membrane permeability parameters. Fig. 5C shows the corresponding νH_2O versus temperature plots. Ice nucleation at high subzero temperatures causes a gradual increase in H_2O band area. At high nucleation temperatures, the H_2O band area ($A\nu H_2O$) at −30 °C is greater compared to nucleation at low subzero temperatures. This 'extra ice' likely comes from the extreme loss of lipid hydration under dehydrating freezing conditions resulting in a greater amount of ice formed in the sample [13]. Fig. 5D depicts an Arrhenius plot of the Lp values obtained from H_2O band analysis. This yields a higher activation energy $E_{Lp,subzero,free\ water}$ of 58.5 kcal mol^{-1} compared to νCH_2 band analysis. The extrapolated Lpg value determined from H_2O band analysis, $Lpg_{subzero,free\ water}$ of 0.0116 μm min^{-1} atm^{-1}, is similar compared to $Lpg_{subzero,bound\ water}$. The two kinetic processes likely denote transport of free and membrane bound water, which was also observed for stallion sperm [14]. In the presence of DMSO, $E_{Lp,subzero,free\ water,DMSO}$ and $Lpg_{subzero,free\ water,DMSO}$ were determined to be 34.2 kcal mol^{-1} and 0.0152 μm min^{-1} atm^{-1}, respectively. Table 2 summarizes the obtained E_{Lp} and Lp values. DMSO particularly affects the transport of membrane bound water.

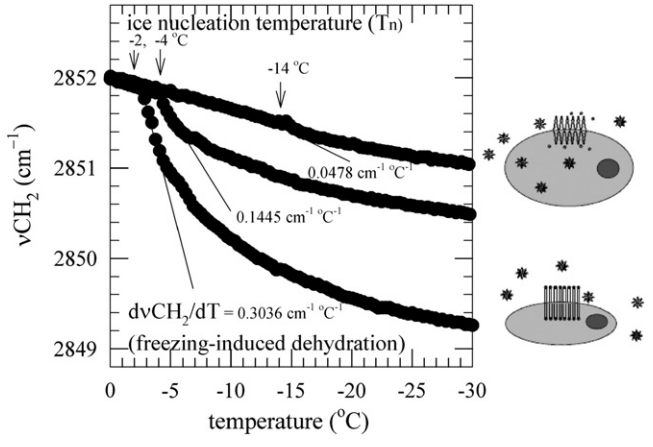

Fig. 4. Membrane phase behavior of 3T3 cells that were cooled from 20 °C to −40 °C at a cooling rate of 1 °C min^{-1} with various ice nucleation temperatures. The data points reflect the shift in band position of the symmetric CH_2 stretching band ($\Delta\nu CH_2$) from 0 to −30 °C. Freezing-induced membrane dehydration ($d\nu CH_2/dT$) as well as Tn is indicated for the different nucleation conditions. The cartoons illustrate that high subzero nucleation temperature cause cellular dehydration and gel phase formation in the membranes. If cellular dehydration does not occur during freezing, membrane stay relatively hydrated.

3.6. Suprazero versus subzero membrane permeability parameters

Fig. 6 shows an Arrhenius plot of the membrane hydraulic permeability at supra and subzero temperatures in the absence of cryoprotective agents. The activation energy for water transport at suprazero temperatures (black filled squares) is smaller compared to that at subzero temperatures in the ice phase for both membrane bound (open squares) as well as free (gray filled squares) water. The extrapolated Lpg value from the suprazero measurements is about 5 fold greater compared to the extrapolated Lpg values from the subzero measurements.

4. Discussion

To model the cryobiological response of a given cell type, the membrane permeability characteristics of the cell need to be experimentally determined. Membrane permeability characteristics are often measured at suprazero temperatures and the measured values are used to predict the response at subzero temperatures. This procedure, however, leads to discrepancies in prediction of cryobiological outcomes [22]. Subzero permeability measurements are usually experimentally difficult and are therefore infrequently reported [23]. Therefore, the development of new methods to study subzero membrane properties of cells is urgently needed in this field of research.

Electronic particle cell size measurements have been used previously to determine the membrane permeability characteristics of cells at suprazero temperatures [24–26]. The observed E_{Lp} at suprazero temperatures suggest that water transport mostly occurs by diffusion through the membrane bilayer rather than through

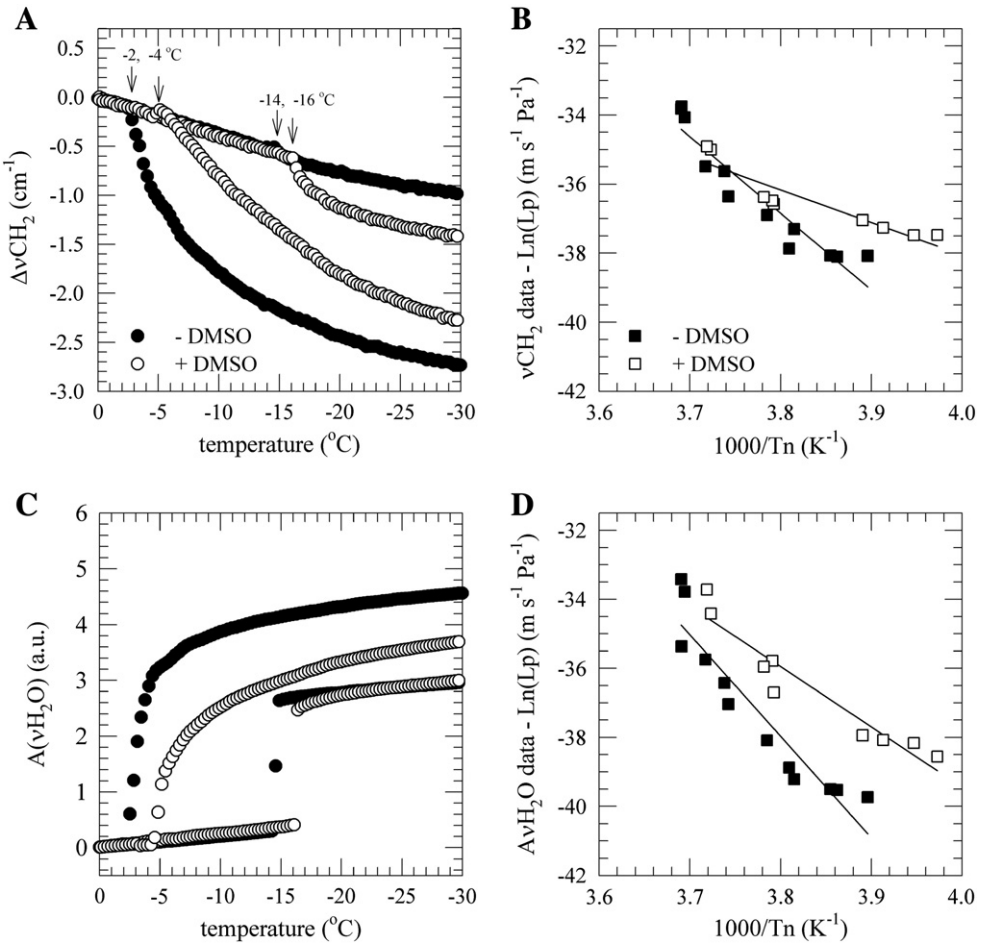

Fig. 5. Membrane phase behavior of 3T3 cells that were cooled from 20 °C to −40 °C at a cooling rate of 1 °C min^{-1} with various ice nucleation temperatures in the absence (filled circles) and presence (open circles) of DMSO. Ice formation was monitored by plotting the area of the H_2O-libration and -bending band as a function of the temperature (C). Panels B and D show Arrhenius plots of the membrane hydraulic permeability (Lp), as derived from νCH_2 band (B) and νH_2O band (D) analysis in the absence (filled squares) and presence (open squares) of DMSO.

channel proteins. Water transport by solubility-diffusion in a lipid-bilayer is characterized by a high Arrhenius activation energy (Ea>10 kcal mol^{-1}), whereas channel-mediated water transport appears to be characterized by a lower Arrhenius activation energy (<6 kcal mol^{-1}) (reference 24 and reference therein).

Lp values determined at suprazero temperatures are typically higher than those determined at subzero temperatures [27], but this has not been investigated in a systematic manner and the database is limited. Here, we show that Lp values obtained at suprazero temperatures cannot be used to estimate the membrane hydraulic permeability in the presence of ice. The differences in the Arrhenius relationship of Lp at supra and subzero temperatures are related to the drastic effects of ice formation on membrane phase state, which affect the membrane hydraulic permeability. The increased subzero E_{Lp} implies that there is reduced water movement at lower temperatures because lipid packing is tighter in the gel phase and water molecules encounter a more hydrophobic environment when crossing the

Table 2
Membrane permeability parameters (E_{Lp} and Lpg) of 3T3 cells. Membrane parameters at suprazero temperatures were determined by Coulter counter measurements. Subzero values of E_{Lp} and Lpg were determined by FTIR from νCH_2 and $A\nu H_2O$ versus temperature plots. Parameters derived from νCH_2 band analysis are referred to as bound water, and those determined from $A\nu H_2O$ band analysis as free water. Parameters were derived from Arrhenius plots in which Ln(Lp) was plotted as a function of the inverse of the nucleation temperature.

	E_{Lp} (kcal mol^{-1})	Lpg (μm min^{-1} atm^{-1})
Suprazero	15.0	0.0631
Subzero, bound water	44.1	0.0130
Subzero, free water	58.5	0.0116
Subzero, bound water, DMSO	18.7	0.0044
Subzero, free water, DMSO	34.2	0.0152

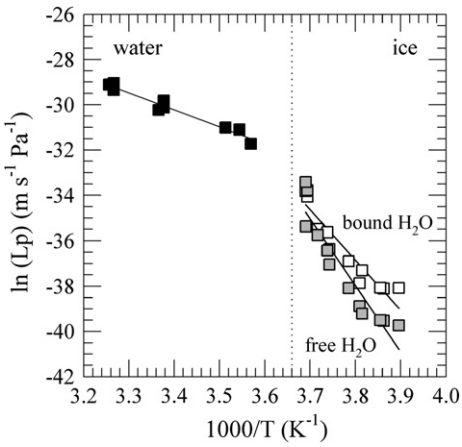

Fig. 6. Combined Arrhenius plot of the membrane permeability of 3T3 cells to water (Lp) at supra and subzero temperatures. The data points reflect the membrane hydraulic permeability (Lp), as determined by Coulter measurements at suprazero temperature (black filled squares) and as determined by FTIR from νCH_2 band (gray filled squares) and νH_2O band (open squares) analysis at subzero temperatures.

membrane. E_{Lp} values for 3T3 cells are in the same order of magnitude as those of various other mammalian cell types determined by cryomicroscopy [13,28,29]. The Lpg value determined here by FTIR for 3T3 cells, however, is lower compared to these cryomicroscopy results. This is likely due to the differences in experimental methodology. By FTIR, Lpg is determined from an Arrhenius plot of Lp determined at various subzero temperatures, whereas cryomicroscopy relies on least squares fitting of the water transport equations through cell dehydration curves obtained at various cooling rates. With cryomicroscopy, the cooling rate strongly affects the obtained permeability parameters and therefore combined fit results are often reported [28,29]. Furthermore, the sample preparation method will have an effect on the parameters. With cryomicroscopy, single cells are measured, whereas for FTIR (and also for DSC) measurements, cell pellets are needed.

The freezing-induced membrane phase transition that is observed at high nucleation temperatures has been observed in a variety of mammalian cell types and is different from the thermotropic phase transitions that occur upon cooling and re-warming of cells at suprazero temperatures (i.e. reference 30). Freezing-induced phase transitions are highly cooperative and depend on the cell-specific membrane lipid composition. The different transport kinetics of membrane bound and free water during freezing have been previously observed in LnCAP tumor cells and in sperm [13,14]. This seems to be a general phenomenon. The freezing-induced gel phase formation at high nucleation temperatures is due to dehydration of the bound water around the phospholipid head groups [12]. This bound water participates in the extracellular ice phase and coincides with additional ice formation in the sample [13]. If cells do not dehydrate during freezing, membranes stay relatively hydrated and the lipid conformational disorder remains relatively high.

Interestingly, DMSO does not prevent fluid-to-gel membrane phase changes during freezing. The phase transition in the presence of DMSO, however, occurs over a wider temperature range (is less cooperative). Similar observations were made with glycerol [14]. This suggests that cells have more time to respond osmotically upon extracellular ice formation in the presence of cryoprotective agents. DMSO particularly affects the transport of membrane bound water during freezing and reduces the activation energy for water transport.

Taken together, subzero membrane permeability characteristics cannot be extrapolated from suprazero measurements stressing the need to develop methods to study membrane properties at subzero temperatures in the presence of ice. The membrane hydraulic permeability is dependent on intrinsic cell properties and can be influenced by cryoprotective agents.

Acknowledgments

This work was financially supported by the German Research Foundation (Deutsche Forschungsgemeinschaft, DFG), Cluster of Excellence 'From regenerative biology to reconstructive therapy' (REBIRTH).

References

[1] P. Mazur, Freezing of living cells: mechanisms and implications, Am. J. Physiol. 247 (1984) C125–C142.
[2] P. Mazur, Kinetics of water loss from cells at subzero temperatures and the likelihood of intracellular freezing, J. Gen. Physiol. 47 (1963) 347–369.
[3] R.L. Levin, E.G. Cravalho, C.E. Huggins, A membrane model describing the effect of temperature on the water conductivity of erythrocyte membranes at subzero temperatures, Cryobiology 13 (1976) 415–429.
[4] M. Toner, E.G. Cravalho, D.R. Armant, Water transport and estimated transmembrane potential during freezing of mouse oocytes, J. Membr. Biol. 115 (1990) 261–272.
[5] K.R. Diller, Quantitative low temperature optical microscopy of biological systems, J. Microsc. 126 (1982) 9–28.
[6] A. Hubel, J. Norman, T.B. Darr, Cryobiophysical characteristics of genetically modified hematopoietic progenitor cells, Cryobiology 38 (1999) 140–153.
[7] S.L. Stott, J.O.M. Karlsson, Visualization of intracellular ice formation using high-speed video cryomicroscopy, Cryobiology 58 (2009) 84–95.
[8] R.V. Devireddy, D. Raha, J.C. Bischof, Measurement of water transport during freezing in cell suspensions using a differential scanning calorimeter, Cryobiology 36 (1998) 124–155.
[9] R.V. Devireddy, D.J. Swanlund, T. Olin, W. Vincente, M.H.T. Troedsson, J.C. Bischof, K.P. Roberts, Cryopreservation of equine sperm: optimal cooling rates in the presence and absence of cryoprotective agents determined using differential scanning calorimetry, Biol. Reprod. 66 (2002) 222–231.
[10] R.V. Devireddy, G. Li, S.P. Leibo, Suprazero cooling conditions significantly influence subzero permeability parameters of mammalian ovarian tissue, Mol. Reprod. Dev. 73 (2006) 330–341.
[11] R. Alapati, M. Stout, J. Saenz, G.T. Gentry Jr., R.A. Godke, R.V. Devireddy, Comparison of the permeability properties and post-thaw motility of ejaculated and epididymal bovine spermatozoa, Cryobiology 59 (2009) 164–170.
[12] W.F. Wolkers, S.K. Balasubramanian, E.L. Ongstad, J.C. Bischof, Effects of freezing on membranes and proteins in LNCaP prostate tumor cells, Biochim. Biophys. Acta: Biomembr. 1768 (2007) 728–736.
[13] S.K. Balasubramanian, W.F. Wolkers, J.C. Bischof, Membrane hydration correlates to cellular biophysics during freezing in mammalian cells, Biochim. Biophys. Acta 1788 (2009) 945–953.
[14] H. Oldenhof, K. Friedel, H. Sieme, B. Glasmacher, W.F. Wolkers, Membrane permeability parameters for freezing of stallion sperm as determined by Fourier transform infrared spectroscopy, Cryobiology 61 (2010) 115–122.
[15] J.H. Crowe, F.A. Hoekstra, L.M. Crowe, T.J. Anchordoguy, E. Drobnis, Lipid phase transitions measured in intact cells with Fourier transform infrared spectroscopy, Cryobiology 26 (1989) 76–84.
[16] W.F. Wolkers, L.M. Crowe, N.M. Tsvetkova, F. Tablin, J.H. Crowe, In situ assessment of erythrocyte membrane properties during cold storage, Mol. Membr. Biol. 19 (2002) 59–65.
[17] D.J. Moore, R.H. Sills, N. Patel, R. Mendelsohn, Conformational order of phospholipids incorporated into human erythrocytes: an FTIR spectroscopy study, Biochemistry 35 (1996) 229–235.
[18] W.F. Wolkers, Biomedical FTIR spectroscopy of lipids, in: BarthA. , HarisP.I. (Eds.), Biological and Biomedical Infrared Spectroscopy, ISBN: 978-1-60750-045-2, 2009, pp. 272–287.
[19] T. Arakawa, S.N. Timasheff, The stabilization of proteins by osmolytes, Biophys. J. 47 (1985) 411–414.
[20] M.H. Jacobs, D.R. Stewart, A simple method for the quantitative measurement of cell permeability, J. Cell. Comp. Physiol. 1 (1932) 71–82.
[21] J.O. Karlsson, E.G. Cravalho, I.H. Borel Rinkes, R.G. Tompkins, M.L. Yarmush, M. Toner, Nucleation and growth of ice crystals inside cultured hepatocytes during freezing in the presence of dimethyl sulfoxide, Biophys. J. 65 (1993) 2524–2536.
[22] P. Mazur, W.F. Rall, S.P. Leibo, Kinetics of water loss and the likelihood of intracellular freezing in mouse ova. Influence of the method of calculating the temperature dependence of water permeability, Cell. Biophys. 6 (1984) 197–213.
[23] F.W. Kleinhans, P. Mazur, Determination of the water permeability (Lp) of mouse oocytes at −25 °C and its activation energy at subzero temperatures, Cryobiology 58 (2009) 215–224.
[24] H.Y. Elmoazzen, J.A.W. Elliott, L.E. McGann, The effect of temperature on membrane hydraulic conductivity, Cryobiology 45 (2002) 68–79.
[25] J.A. Gilmore, L.E. McGann, J. Liu, D.Y. Gao, A.T. Peter, F.W. Kleinhans, J.K. Crister, Effect of cryoprotectant solutes on water permeability of human spermatozoa, Biol. Reprod. 53 (1995) 985–995.
[26] L.E. McGann, J.M. Turc, Determination of water and solute permeability coefficients, Cryobiology 17 (1980) 612–613.
[27] H. Sieme, R.A.P. Harrison, A.M. Petrunkina, Cryobiological determinants of frozen semen quality, with special reference to stallion, Anim. Reprod. Sci. 107 (2008) 276–292.
[28] S.K. Balasubramanian, J.C. Bischof, A. Hubel, Water transport and IIF parameters for a connective tissue equivalent, Cryobiology 52 (2006) 62–73.
[29] S.K. Balasubramanian, R.T. Venkatasubramanian, A. Menon, J.C. Bischof, Thermal injury prediction during cryoplasty through in vitro characterization of smooth muscle cell biophysics and viability, Ann. Biomed. Eng. 36 (2008) 86–101.
[30] J.C. Bischof, W.F. Wolkers, N.M. Tsvetkova, A.E. Oliver, J.H. Crowe, Lipid and protein changes due to freezing in Dunning AT-1 cells, Cryobiology 45 (2002) 22–32.